PHYSICAL REVIEW B **95**, 180410(R) (2017)

Thermodynamically stable skyrmion lattice at low temperatures in a bulk crystal of lacunar spinel GaV_4Se_8

Y. Fujima, N. Abe, Y. Tokunaga, and T. Arima
Department of Advanced Materials Science, University of Tokyo, Kashiwa 277-8561, Japan
(Received 10 November 2016; published 30 May 2017)

The magnetic field–temperature (H-T) phase diagram of a lacunar spinel GaV_4Se_8 is determined by means of ac magnetic susceptibility and magnetoelectric measurements on single crystals and classical Monte Carlo simulation. GaV_4Se_8 is pyroelectric below the structural phase transition temperature $T_S = 41$ K and magnetically ordered below $T_C = 17.5$ K. Ac magnetic susceptibility measurement has revealed that GaV_4Se_8 undergoes successive magnetic phase transitions with increasing applied magnetic field. Each phase is assigned to cycloidal, skyrmion lattice, and forced ferromagnetic phases. Both cycloidal and skyrmion-lattice magnetic orders induce electric polarization up to around 10 $\mu C/m^2$ compared with ferromagnetic order, suggesting a spin-driven magnetoelectric nature in GaV_4Se_8. The skyrmion lattice phase seems to be stable down to $T = 2$ K and up to $\mu_0 H = 370$ mT. This enhanced stability of skyrmion lattice in GaV_4Se_8 compared with GaV_4S_8 may provide a key to understanding the formation mechanism of the skyrmion lattice.

DOI: 10.1103/PhysRevB.95.180410

In noncentrosymmetric magnetic crystals, a uniform antisymmetric exchange interaction called the Dzyaloshinskii-Moriya interaction is allowed [1,2]. If the exchange interaction between two neighboring moments is ferromagnetic, the uniform antisymmetric interaction competes with the ferromagnetic exchange interaction, resulting in the formation of noncollinear magnetic structures. Magnetic skyrmions, topologically protected nanoscale spin structures, are typical examples [3]. They have been attracting a lot of attention due to their potential application for spintronic devices [4]. Skyrmions have been known to form a lattice structure in chiral magnetic crystals such as MnSi [5,6], Cu_2OSeO_3 [7], Co-Zn-Mn alloy [8], and so on. Ferromagnetic exchange interactions and the uniform antisymmetric exchange interactions are essential to stabilize the skyrmion lattice in chiral magnets. A similar uniform antisymmetric exchange interaction is also found in a polar system [9]. A Néel-type magnetic skyrmion lattice phase was first observed on a Fe monatomic layer on the Ir surface [10]. More generally, Bogdanov and Yablonskii predicted that Néel-type magnetic skyrmions can be formed in the magnetic crystals belonging to the crystallographic classes C_{nv} [11]. In fact, Néel-type skyrmion lattice in bulk crystal was reported in a polar achiral lacunar spinel GaV_4S_8 [12,13]. The Néel-type skyrmion lattice was observed down to 8.9 K ($\sim 0.68 T_C$). In chiral crystals, the orientations of magnetic propagation vectors are not determined by the Dzyaloshinskii-Moriya interaction [5,7]. In polar crystals, on the other hand, they are restricted to lie perpendicular to the direction of crystallographic polarization [12]. Furthermore, possibly competing phases with the skyrmion lattice phase are longitudinal helix/cone in the chiral magnets, while the relevant helices and cones are of cycloidal type in the polar magnets. These differences should affect the stability of skyrmion lattices.

In GaM_4X_8 (M = V,Mo; X = S,Se), M ions form a breathing pyrochlore network reflecting the periodic deficiencies of Ga ions in A sites of conventional spinel structure [14–20]. The crystal structure is also regarded as the rocksalt-type binary structure composed of $(M_4X_4)^{5+}$ and $(GaX_4)^{5-}$ with a noncentrosymmetric cubic space group $F\bar{4}3m$ at room temperature. M ions are responsible for their magnetizations with $S = 1/2$ per $(M_4X_4)^{5+}$ cluster. At low temperatures, they undergo Jahn-Teller-type structural phase transition to a polar $R3m$ phase accompanied by the elongation along one of the $\langle 111 \rangle$ axes in the cubic setting. In this polar phase, there work ferromagnetic interactions between neighboring $(M_4X_4)^{5+}$ clusters. The exchange interactions may compete with Dzyaloshinskii-Moriya interactions caused by the polar structure, and result in noncollinear magnetic structures. In addition, the physical parameters in this system could be modulated by the element substitutions of M sites and X sites. Therefore, this system provides a good platform to investigate the effects of the modulation of physical parameters on a skyrmion lattice in polar crystals. However, there is no report on the physical properties for GaM_4X_8 single crystals except GaV_4S_8 [12,13,21–24] up to now.

In this Rapid Communication, we report the magnetic field–temperature (H-T) phase diagram of a lacunar spinel GaV_4Se_8 using single crystals. GaV_4Se_8 undergoes the structural phase transition to a polar space group $R3m$ at $T_S = 41$ K. Magnetic moments of V ions were considered to order ferromagnetically below $T_C = 18$ K in a previous study using polycrystalline samples [20]. The substitution of Se for S modulates the transfer integrals and spin-orbit coupling, and may affect the stability of the skyrmion lattice. In fact, we observed a skyrmion lattice phase down to 2 K ($\sim 0.1 T_C$) in GaV_4Se_8.

Single crystals of GaV_4Se_8 were grown by the chemical vapor transport method. Starting materials were gallium ingots, vanadium flakes, and selenium grains. Polycrystalline GaV_4Se_8 was prepared by reacting stoichiometric mixtures of the elements in an evacuated silica tube at 950 °C for 24 h. The reaction products were ground and sealed in an evacuated silica tube with $PtCl_2$ as the transport agent, and heated in a two-zone furnace. Both ends of the tube were kept at 960 °C and 920 °C for 360 h, respectively. Obtained single crystals were characterized by single crystal x-ray diffraction. Magnetization was measured by using a superconducting quantum interference device (Quantum Design MPMS-XL).

The dielectric constant was measured by using an LCR meter (Agilent E4980A). The change in electric polarization as a function of magnetic field was calculated by integrating displacement current while sweeping magnetic field with respect to time. The displacement current was measured by using an electrometer (Keithley 6517B). To align the polar domains created at the structural phase transition, the single crystalline sample was cooled in both a magnetic field $H_{\rm pol}$ and a poling electric field $E_{\rm pol}$ along the [111] axis, which are typically $\mu_0 H_{\rm pol} = 8$ T and $E_{\rm pol} = 1.7$ kV/cm, respectively [25]. The poling electric field was removed before measuring the displacement current. Ac susceptibility was measured by a conventional self-inductance method using a lock-in amplifier (NF Corporation LI5640). The frequency of the excitation magnetic field was 523 Hz.

Classical Monte Carlo simulation was performed for a two-dimensional triangular-lattice spin system. The Hamiltonian $\mathcal{H}$ is described as

$$\mathcal{H} = \mathcal{H}_{\rm ex} + \mathcal{H}_{\rm DM} + \mathcal{H}_{\rm Zeeman},$$

$$\mathcal{H}_{\rm ex} = -\sum_{\langle i,j\rangle} \left(J_\perp m_i^x m_j^x + J_\perp m_i^y m_j^y + J_\parallel m_i^z m_j^z\right),$$

$$\mathcal{H}_{\rm DM} = \sum_{\langle i,j\rangle} \boldsymbol{D}_{ij} \cdot (\boldsymbol{m}_i \times \boldsymbol{m}_j),$$

$$\mathcal{H}_{\rm Zeeman} = -H \sum_i m_i^z,$$

where $\boldsymbol{m}_i$ represents a magnetic moment on site i. The Cartesian coordinate system is defined so that z is parallel to the polar axis. Here, a ferromagnetic exchange interaction with XXZ-type anisotropy ($J_\perp, J_\parallel$) is assumed, considering the uniaxial anisotropy in the $R3m$ system. The Dzyaloshinskii-Moriya vectors $\boldsymbol{D}_{ij}$ are parallel to the lattice plane and perpendicular to each bond, taking into account the crystallographic threefold symmetry along the [111] axis. Magnetic field H is applied along the z axis. $|\boldsymbol{D}|/J_\perp = 1$ and $J_\parallel/J_\perp = 1.08$ for the calculations. The system was a regular hexagon with a side of 32 sites. Electric dipole moment $\Delta \boldsymbol{p}_{ij}$ on each bond was calculated by using the spin-current mechanism $\Delta \boldsymbol{p}_{ij} \propto \boldsymbol{e}_{ij} \times (\boldsymbol{m}_i \times \boldsymbol{m}_j)$ [26], where $\boldsymbol{e}_{ij}$ is the unit vector connecting the sites i and j.

The grown single crystals were black and of tetrahedral shape with a side of around 1 mm, as shown in Fig. 1(b). The triangular planes are indexed as {111} in the cubic setting. Figure 1(c) shows the temperature dependence of pyrocurrent, dielectric permittivity, and magnetization along the polar [111] axis. Pyrocurrent shows a sharp peak and dielectric permittivity exhibits a jump at $T_{\rm S} = 41$ K, indicating a pyroelectric phase transition. It should be noted that the apparent temperature dependence of the pyrocurrent comes in part from the change of the resistivity. Associated with the pyroelectric phase transition, inverse magnetic susceptibility shows a jump. The Curie-Weiss temperature is $\theta_{\rm CW} = -84.6$ K for $T > T_{\rm S}$ and $\theta_{\rm CW} = 20.8$ K for $T < T_{\rm S}$. This indicates that the exchange interaction between magnetic moments of V ions changes from antiferromagnetic to ferromagnetic at the pyroelectric phase transition. The ferroic ordering in the $(V_4Se_4)^{5+}$ cluster orbital degree of freedom below $T_{\rm S}$ may change the exchange interaction between neighboring clusters

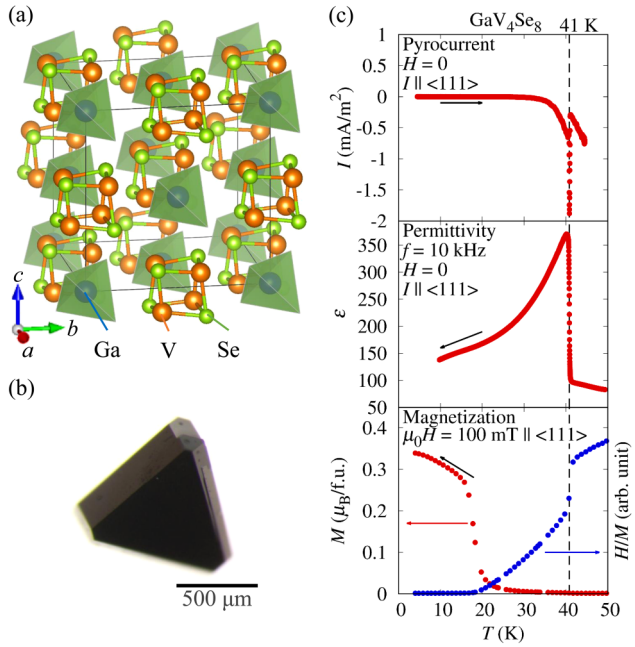

FIG. 1. (a) Crystal structure of GaV_4Se_8 at room temperature with the cubic space group $F\bar{4}3m$ drawn by VESTA software [27]. Blue, orange, and green balls represent Ga, V, and Se atoms, respectively. (b) An obtained single crystal of GaV_4Se_8 with a tetrahedral shape. The scale bar indicates 500 μm. (c) Pyrocurrent, permittivity, and magnetization along the [111] axis in the cubic setting as a function of temperature for GaV_4Se_8. Typical sweeping rate for pyrocurrent measurement is 0.08 K/s. Magnetization was measured in applied magnetic field $\mu_0 H = 100$ mT. Inverse susceptibility is plotted by blue circles. A vertical dashed line at $T = 41$ K is a guide for the eyes.

into ferromagnetic. Magnetization shows a steep change at $T_{\rm C} = 17.5$ K reflecting ferromagnetic order of magnetic moments of V ions in agreement with the previous work on the polycrystalline sample [20].

Figure 2(a) shows magnetization, the real part of ac susceptibility χ', and electric polarization as a function of applied magnetic field along the [111] axis at $T = 13$ K. Magnetization exhibits a jump and χ' shows a peak at $\mu_0 H = 70$ mT. The χ' value shows a steep change at $\mu_0 H = 370$ mT, above which the magnetization is almost saturated. These behaviors indicate successive magnetic phase transitions. In the saturated state, a $(V_4Se_4)^{5+}$ cluster induces $0.7\mu_{\rm B}$, which is roughly consistent with the picture of $(V_4Se_4)^{5+}$ clusters with $S = 1/2$ as a result of the formation of cluster orbitals. The deviation may be attributable to the presence of orbital current. Accompanied by the magnetic phase transitions, electric polarization also changes by the order of 10 μC/m^2. This suggests that magnetic order should couple with electric polarization. By taking into account the poling-field dependence of χ' and electric polarization, it is confirmed that a small anomaly at $\mu_0 H = 150$ mT arises from minor crystallographic trigonal domains created at $T_{\rm S}$ (discussed in the Supplemental Material [28]).

To understand the magnetic order in each phase, one must consider exchange interaction, Dzyaloshinskii-Moriya

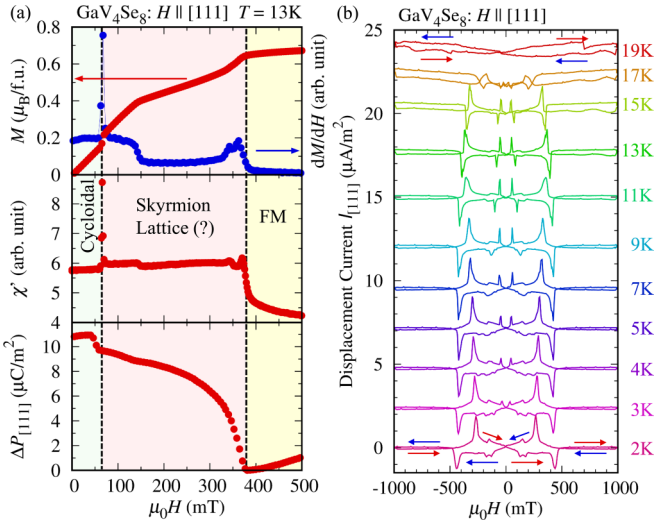

FIG. 2. (a) Magnetization M, the real part of ac susceptibility χ', and induced electric polarization $\Delta P_{[111]}$ along the [111] axis as a function of applied magnetic field H along the [111] axis at $T = 13$ K. Derivative of magnetization with respect to the magnetic field is plotted by blue circles. Vertical dashed lines are a guide for the eyes. (b) Displacement current $I_{[111]}$ along the [111] axis with sweeping the applied magnetic field along the [111] axis at various temperatures. The typical sweeping rate is 8 mT/s. The baselines are shifted for clarity.

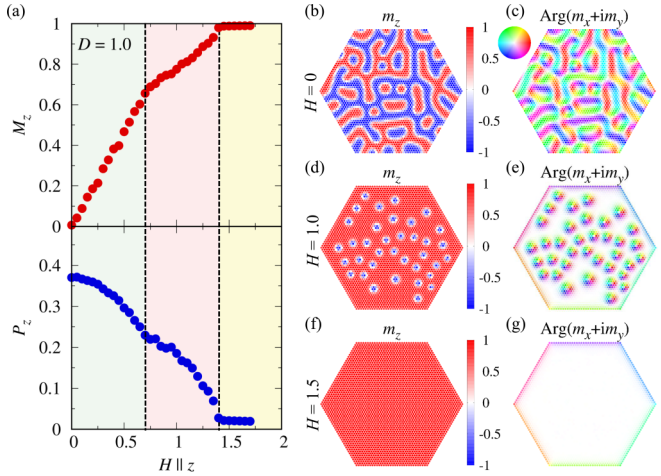

FIG. 3. The result of classical Monte Carlo simulations on Heisenberg spins on two-dimensional triangular lattice (see text). (a) Magnetization and electric polarization perpendicular to the lattice plane as a function of magnetic field. (b)–(g) Magnetic moment arrangements obtained by the simulation in $H = 0$, 1.0, and 1.5. In (b), (d), and (f), the out-of-plane component of the magnetic moments is mapped by color. Red and blue colors correspond to the directions parallel and antiparallel to the magnetic field, respectively. In (c), (e), and (g), the direction of in-plane components of the magnetic moments is represented by the color wheel.

interaction, and Zeeman energy. At zero magnetic field, cycloidal order is expected to be stabilized by the competition between the exchange interaction and the Dzyaloshinskii-Moriya interaction. On the other hand, forced ferromagnetic order is the most stable in high magnetic field limit to gain Zeeman energy. Between these phases, magnetic skyrmions or solitons could emerge and form a lattice. Here, in contrast to a chiral magnet, a conical magnetic phase could not be stabilized in a magnetic field along the polar axis. In our magnetization measurement, magnetization shows a jump at the transition between the cycloidal and the intermediate phase. Therefore, the intermediate phase should likely be a skyrmion lattice phase, which could not be made from cycloidal structure by continuous deformations.

Figure 2(b) shows magnetoelectric effect at various temperatures between $T = 2$ K and $T = 19$ K. The vertical axis is displacement current along the [111] axis with the applied magnetic field sweeping along the [111] axis, which roughly corresponds to $dP_{[111]}/dH$. The magnetoelectric signal was observed even in the paramagnetic phase at $T = 19$ K. A possible origin is the magnetostriction, which may result in the change of the electric polarization. On the other hand, displacement current shows peaks below T_C. These peaks correspond to the magnetic transitions determined from the ac susceptibility measurement. Therefore, the nonlinear magnetoelectric effect is expected to arise from the emergence of the cycloidal structure or skyrmion lattice. This feature is observed down to $T = 2$ K which is the lowest temperature in our experiment. This suggests that the intermediate phase is stable even at the lowest temperature in contrast to the case in GaV_4S_8 [12]. Magnetization (not shown) and magnetoelectric effect show hysteretic behaviors as a function of magnetic field at low temperatures, suggesting the bistability between competing magnetic structures.

Figure 3(a) shows calculated magnetization M_z and electric polarization P_z perpendicular to the lattice plane as a function of the applied magnetic field H. Magnetization shows an anomaly at $H = 0.7$ and saturated above $H = 1.4$. Figure 3 shows [(b),(d),(f)] out-of-plane and [(c),(e),(g)] in-plane components of the magnetic moments. At $H = 0$, a rather short-range cycloidal structure is formed [Figs. 3(b) and 3(c)]. Upon increasing the magnetic field, Néel-type magnetic skyrmions are created [Figs. 3(d) and 3(e)], and then finally changed to the forced ferromagnetic state [Figs. 3(f) and 3(g)]. Electric polarization calculated by a spin-current mechanism is the largest at $H = 0$ and decreases down to zero by increasing the magnetic field. These behaviors are qualitatively consistent with our experimental results shown in Fig. 2(a), while the exchange striction model was considered in the previous study on GaV_4S_8 [22]. Because any magnetostriction was not taken into account in this calculation, the magnetoelectric effect observed in the saturated state could not be reproduced.

Figure 4 shows the entire H-T phase diagram of GaV_4Se_8 with decreasing external magnetic field $H \parallel [111]$ determined from the present ac susceptibility and magnetoelectric measurements using single crystals. GaV_4Se_8 is pyroelectric below $T_S = 41$ K and magnetically ordered below $T_C = 17.5$ K. As the magnetic field increases, the magnetic state changes from cycloidal to skyrmion lattice and finally to forced ferromagnetic state. In GaV_4Se_8, noncollinear magnetic structures such as cycloid and skyrmion lattice are stable in a larger temperature and magnetic field region than in GaV_4S_8 [12], as described quantitatively below. The saturation magnetic

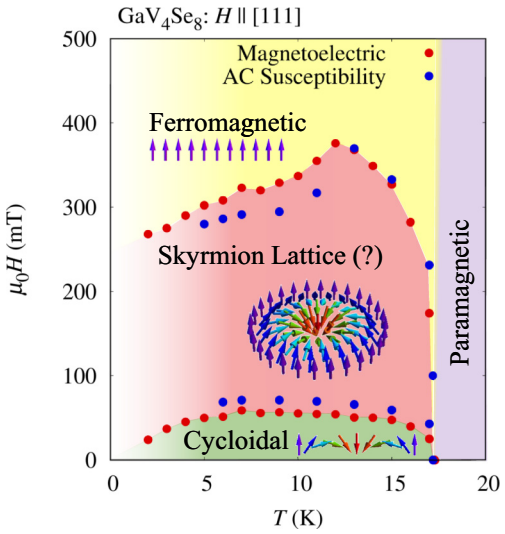

FIG. 4. The *H*-*T* phase diagram of GaV_4Se_8 with external magnetic field along the polar axis [111] determined by ac susceptibility and magnetoelectric measurements using single crystals. Each magnetic structure is schematically shown.

field H_{sat} of GaV_4Se_8 is 5.3 times as large as that of GaV_4S_8 ($H_{sat}^{GaV_4Se_8}/H_{sat}^{GaV_4S_8} = 5.3$). The ratio of magnetic ordering temperature T_C of GaV_4Se_8 to that of GaV_4S_8 ($T_C^{GaV_4Se_8}/T_C^{GaV_4S_8}$) is 1.4. Furthermore, in GaV_4Se_8, the skyrmion lattice phase seem to be stable even at the lowest temperature, while skyrmion lattices in other noncentrosymmetric bulk systems have been observed only near the magnetic ordering temperatures [5,7,8,12].

The saturation behavior in applied magnetic field perpendicular to the Dzyaloshinskii-Moriya vector is well studied for the one-dimensional spin chain system [29–31]. The saturation magnetic field is given by $H_{sat} \simeq (\pi D/4J)^2 JS \propto D^2/J$. Since the magnetic ordering temperature is predicted to be proportional to J by the mean-field theory, one can get the relation $D/J \propto \sqrt{H_C/T_C}$. By using this relation, D/J of GaV_4Se_8 is estimated to be twice as large as that of GaV_4S_8. The magnitude of the Dzyaloshinskii-Moriya vector is given by $|D| \simeq |J(\lambda\Delta E)|$ [2], where λ and ΔE represent the spin-orbit coupling constant and the energy gaps between ground state and excited states, respectively. According to *ab initio* calculations for density of state of GaV_4S_8 and GaV_4Se_8, $\Delta E^{GaV_4S_8}/\Delta E^{GaV_4Se_8} = 1.1$ [32]. Therefore, spin-orbit coupling in GaV_4Se_8 is estimated to be approximately twice as strong as that in GaV_4S_8. This strong spin-orbit interaction caused by element substitution of Se sites likely stabilizes the skyrmion lattice phase.

In conclusion, we establish the *H*-*T* phase diagram of GaV_4Se_8 by ac susceptibility and magnetoelectric measurements using single crystals combined with classical Monte Carlo simulations. In contrast to the case of GaV_4S_8 [12], noncollinear magnetic structures such as cycloidal helix and skyrmion lattice are stable down to $T = 2$ K and up to $\mu_0 H = 370$ mT in GaV_4Se_8. This is likely related to the enhancement of spin-orbit coupling caused by the elemental substitution of Se sites. These noncollinear magnetic structures induce electric polarization possibly by a spin current mechanism. The bistability at the phase boundary and excess polarizations in these magnetic phases may enable the nonvolatile control of skyrmions by an electric field.

We acknowledge fruitful discussions with Y. Nii, H. Sagayama, and K. Matsuura. This work was supported by a Grant-In-Aid for Challenging Exploratory Research (Grant No. 16K13828) from Japan Society for the Promotion of Science (JSPS). The magnetization and magnetoelectric measurements were carried out using facilities of the Institute for Solid State Physics, the University of Tokyo. Y.F. is supported by JSPS through Program for Leading Graduate Schools (MERIT).

[1] I. Dzyaloshinsky, J. Phys. Chem. Solids **4**, 241 (1958).
[2] T. Moriya, Phys. Rev. Lett. **4**, 228 (1960).
[3] A. Bogdanov and A. Hubert, J. Magn. Magn. Mater. **138**, 255 (1994).
[4] N. Nagaosa and Y. Tokura, Nat. Nanotechnol. **8**, 899 (2013).
[5] S. Mühlbauer, B. Binz, F. Jonietz, C. Pfleiderer, A. Rosch, A. Neubauer, R. Georgii, and P. Böni, Science **323**, 915 (2009).
[6] X. Z. Yu, Y. Onose, N. Kanazawa, J. Park, J. Han, Y. Matsui, N. Nagaosa, and Y. Tokura, Nature (London) **465**, 901 (2010).
[7] S. Seki, X. Z. Yu, S. Ishiwata, and Y. Tokura, Science **336**, 198 (2012).
[8] Y. Tokunaga, X. Z. Yu, J. White, H. M. Rønnow, D. Morikawa, Y. Taguchi, and Y. Tokura, Nat. Commun. **6**, 7638 (2015).
[9] M. Bode, M. Heide, K. Von Bergmann, P. Ferriani, S. Heinze, G. Bihlmayer, A. Kubetzka, O. Pietzsch, S. Blügel, and R. Wiesendanger, Nature (London) **447**, 190 (2007).
[10] S. Heinze, K. Von Bergmann, M. Menzel, J. Brede, A. Kubetzka, R. Wiesendanger, G. Bihlmayer, and S. Blügel, Nat. Phys. **7**, 713 (2011).
[11] A. N. Bogdanov and D. A. Yablonskii, Sov. Phys. JETP **68**, 101 (1989).
[12] I. Kézsmárki, S. Bordács, P. Milde, E. Neuber, L. M. Eng, J. S. White, H. M. Rønnow, C. D. Dewhurst, M. Mochizuki, K. Yanai, H. Nakamura, D. Ehlers, V. Tsurkan, and A. Loidl, Nat. Mater. **14**, 1116 (2015).
[13] J. S. White, Á. Butykai, R. Cubitt, D. Honecker, C. D. Dewhurst, L. F. Kiss, V. Tsurkan, and S. Bordács, arXiv:1704.03621.
[14] R. Pocha, D. Johrendt, and R. Pöttgen, Chem. Mater. **12**, 2882 (2000).
[15] H. Haeuseler, S. Reil, and E. Elitok, Int. J. Inorg. Mater. **3**, 409 (2001).
[16] Y. Sahoo and A. Rastogi, J. Phys.: Condens. Matter **5**, 5953 (1993).
[17] H. Haeuseler and W. Cordes, Z. Naturforsch. B: J. Chem. Sci. **47**, 901 (1992).
[18] M. François, O. Alexandrov, K. Yvon, H. B. Yaich-Aerrache, P. Gougeon, M. Potel, and M. Sergent, Z. Kristallogr. - Cryst. Mater. **200**, 47 (1992).

[19] M. Francois, W. Lengauer, K. Yvon, M. Sergent, M. Potel, P. Gougeon, and H. B. Yaich-Aerrache, Z. Kristallogr. - Cryst. Mater. **196**, 111 (1991).
[20] D. Bichler and D. Johrendt, Chem. Mater. **23**, 3014 (2011).
[21] H. Nakamura, H. Chudo, and M. Shiga, J. Phys.: Condens. Matter **17**, 6015 (2005).
[22] E. Ruff, S. Widmann, P. Lunkenheimer, V. Tsurkan, S. Bordács, I. Kézsmárki, and A. Loidl, Sci. Adv. **1**, e1500916 (2015).
[23] Z. Wang, E. Ruff, M. Schmidt, V. Tsurkan, I. Kézsmárki, P. Lunkenheimer, and A. Loidl, Phys. Rev. Lett. **115**, 207601 (2015).
[24] D. Ehlers, I. Stasinopoulos, V. Tsurkan, H.-A. Krug von Nidda, T. Fehér, A. Leonov, I. Kézsmárki, D. Grundler, and A. Loidl, Phys. Rev. B **94**, 014406 (2016).
[25] It was revealed by our experiments that not only the electric field but also magnetic field along the [111] axis is effective to align the polar domains.
[26] H. Katsura, N. Nagaosa, and A. V. Balatsky, Phys. Rev. Lett. **95**, 057205 (2005).
[27] K. Momma and F. Izumi, J. Appl. Crystallogr. **44**, 1272 (2011).
[28] See Supplemental Material at http://link.aps.org/supplemental/10.1103/PhysRevB.95.180410 for details.
[29] J.-i. Kishine and A. S. Ovchinnikov, Phys. Rev. B **79**, 220405(R) (2009).
[30] J.-i. Kishine, A. S. Ovchinnikov, and I. V. Proskurin, Phys. Rev. B **82**, 064407 (2010).
[31] J.-i. Kishine, I. V. Proskurin, and A. S. Ovchinnikov, Phys. Rev. Lett. **107**, 017205 (2011).
[32] M. Sieberer, S. Turnovszky, J. Redinger, and P. Mohn, Phys. Rev. B **76**, 214106 (2007).